National Conference with International Participation
ENGINEERING MECHANICS 2006
Svratka, Czech Republic, May 15 – 18, 2006
paper no. 290

TRANSIENT TEMPERATURE FIELD IN THE CHAMBER FOR MEASUREMENT OF SURFACE TENSION OF SUPERCOOLED LIQUIDS

J. Hrubý*, M. Müller, K. Richtr, R. Mareš

Summary: *We present results of mathematical modeling of the transient temperature field in a new chamber developed to measure surface tension of supercooled liquids, and results of auxiliary measurements. The chamber is designed to enable a very fast (within 0.1 s) formation of a homogeneous temperature field (within 0.02 K) after a temperature jump of 60 K. The interior of the chamber of dimensions 20x16x32 mm is filled with dry nitrogen surrounding the measuring capillary and thermometers (very fine thermocouples and RTD's). The temperature jump is generated by switching the flow direction of the nitrogen serving as a heat transmitting fluid. To reduce the thermal boundary layer near the bottom and ceiling walls, they are made permeable and some gas is sucked out. The flow in the chamber is laminar. We compute the temperature field analytically and numerically, using the commercial software Fluent. The analytical solution results in a series of goniometric and confluent hyperbolic functions. The Fluent code has been adapted to accept special boundary conditions for the velocity and temperature fields at the permeable walls. The results indicate that the design objectives of the experimental device were met.*

1. Introduction

For a limited time, pure liquids can remain liquid even deep below the freezing point. Liquid below its equilibrium freezing point is metastable and it is called the supercooled liquid. Supercooled liquid water was observed down to 240 K. Surface tension is an important property in case of small droplets, capillary flows etc. It governs the process of nucleation, i.e. formation of droplets. In nucleation experiments, formation of liquid droplets of supercooled water is assumed to take place down to 205 K. Only two datasets [Hacker 1951, Floriano 1990] exist for the surface tension of supercooled water and they are inconsistent. Therefore, a project was started to obtain new measurements. The present contribution describes analysis of the temperature field in the measuring chamber of the device. The surface tension is measured by an original modification of the capillary method. Capillaries has internal diameter ranging from 0.05 to 0.3 mm. The requirement is that within a fraction of second

* Ing. Jan Hrubý, CSc.: Institute of Thermomechanics AS CR, e-mail: hruby@it.cas.cz. Ing. Miloš Müller: Technical University of Liberec. Ing. Karel Richtr and Prof. Ing. Radim Mareš, CSc.: University of West Bohemia in Pilsen

homogeneous temperature field must be established in the chamber, in order that the active length of the capillary and temperature sensors (miniature thermocouples and platinum resistance thermometers) are at the accurate temperature (within 0.02 K). The change of temperature is performed by switching the flow of dry nitrogen, which comes either from left or right, tempered to low temperature or room temperature to melt the ice in case the liquid would freeze.

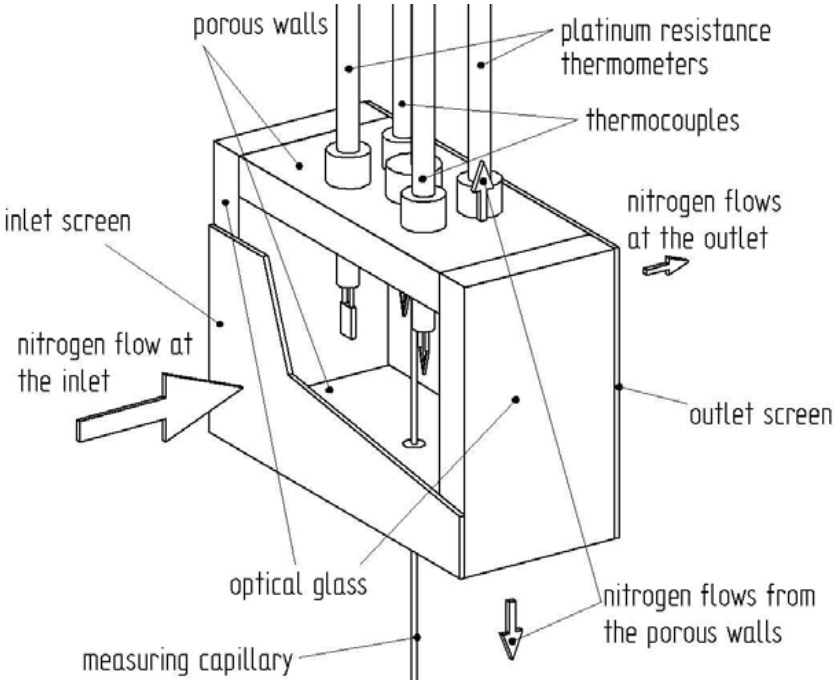

Figure 1. View of the experimental chamber. The relative magnitude of the flows is indicated by the size of the arrows.

2. The new chamber for measurement of surface tension of supercooled liquids

The internal dimensions of the chamber are as follows: length a=16 mm, height b=20 mm, width c=32 mm. Front and back walls are made of optical glass of thickness 4 mm. Upper and lower walls are made of 4 mm thick sintered glass, commercial porosity grade 3.

Flow properties of the sintered glass plates. In the relevant range the pressure drop across the sintered glass plate is linearly proportional to the normal component of the incoming flow velocity. This behavior is a consequence of the creeping flow $\mathrm{Re} \ll 1$ through the pores of the sintered glass. We made measurements of the dependency of the pressure drop across a porosity grade 3 sintered-glass circular plate of diameter 55 mm on the flow rate of air (0 to 15 liters per minute, corresponding to flow velocities 0 to 0.104 m/s at room temperature (20°C) and atmospheric pressure (101325 Pa). The magnitude of the proportionality constant between the pressure drop and normal flow velocity was determined as 5.3×10^4 Pa.s.m^{-1}. Analogous measurements in a lower flow rate range (0 to 2 liters per minute, corresponding to flow velocities 0 to 0.015 m/s) were made for a porosity grade 4

(finer) sintered glass plate of the same dimensions, yielding a proportionality constant of 5.7×10^5 Pa.s.m^{-1}.

Flow properties of the screens. Pressure losses across screens were analyzed by Cornell [Cornell 1958]. In the range 0.006<Re<20 he recommends a correlation by MacDougall [loc.cit.]:

$$\lambda = \frac{33.93}{\mathrm{Re}} \frac{s(1-s)^{-1.27}}{1+(1-s)^{1/2}} \tag{1}$$

where λ is the non-dimensional loss coefficient

$$\lambda \equiv \frac{\Delta p}{\frac{1}{2}\rho v^2}. \tag{2}$$

s is the solidity (or solidity ratio), defined as a ration of blocked area to the total area of the screen, and Re is the Reynolds number, defined as

$$\mathrm{Re} = \frac{v_1 d}{(1-s)\nu_1}. \tag{3}$$

3. Analytical computation of the temperature field

After switching the flow direction, the gaseous content of the chamber is almost instantaneously (in about 0.06 s) exchanged from the warm gas to the cold gas. However, the side-walls glass walls and the upper and lower sintered glass walls still remain at the initial (high) temperature. Compared to the gas, the solid parts have a very high thermal capacity. Heat diffuses from the hot walls into the chamber and deteriorates the temperature field. Therefore, measures are taken to reduce this effect by modifying the flow using the inlet and outlet screens which homogenize the flow and upper and lower permeable plates through which the thermal boundary layer is sucked out. For a relatively long period (seconds) the situation is quasi-stationary—the walls remain at the initial temperature. This is the case which is studied in this contribution.

Because the entrance and outlets of the chamber through materials providing uniform distributions of velocities, we can consider the following boundary conditions. The fluid enters at $x = 0$ with velocity u_0, independent of y and z. At $x = a$ it leaves at velocity u_a, in dependent of y and z. At $y = 0$ and $y = b$ the fluid is sucked out at velocities v_0 and v_b, independent of x and z. At $z = 0$ and $z = c$ the velocity is zero (impermeable wall). Although the normal components of the velocities are nonzero at the permeable walls, the tangential (parallel with the wall) components should vanish. To a sufficient degree of approximation the flow field can be assumed as follows:

$$u = u_0 - qx,\ \ v = v_0 + qy,\ \ w = 0, \tag{4}$$

Here, q is a constant. The flow-field given by Eqs. (4) satisfies the continuity equation and the Navier-Stokes equations. The boundary conditions are satisfied for the normal components of

the velocities. However, the tangential components are nonzero. From the Navier-Stokes equations the pressure field can be determined:

$$p = p_0 + \rho q\left(u_0 x - qx^2/2 + v_0 y + qy^2/2\right). \tag{5}$$

Because the model of the flow field is independent of z, the differential equation of a streamline is given as

$$\frac{dy}{dx} = \frac{v}{u} = \frac{v_0 + qy}{u_0 - qx}. \tag{6}$$

This equation can be easily integrated, showing that the streamlines are hyperbolas:

$$y = \frac{1}{q}\left[\frac{(v_0 + qy_0)(u_0 - qx_0)}{u_0 - qx} - v_0\right]. \tag{7}$$

For the assumed flow field, the equation of energy conservation results in

$$\left(u_0 - qx\right)\frac{\partial T}{\partial x} + \left(v_0 + qy\right)\frac{\partial T}{\partial y} = \kappa\left(\frac{\partial^2 T}{\partial x^2} + \frac{\partial^2 T}{\partial y^2} + \frac{\partial^2 T}{\partial z^2}\right). \tag{8}$$

where κ is thermal diffusivity of the fluid. We constrain further analysis to the symmetric case $v_b = -v_{-b}$, i.e. $v_0 = 0$, $q = v_b / b$. We introduce the following dimensionless quantities:

$$\overline{x} \equiv x/b,\ \overline{y} \equiv y/b,\ \overline{z} \equiv z/b,\ \overline{a} \equiv a/b,\ \overline{c} \equiv c/b,\ \overline{u} \equiv ub/\kappa,\ \overline{v} \equiv vb/\kappa,\ \overline{w} \equiv wb/\kappa, \tag{9}$$

$$\overline{T} \equiv \frac{T - T_1}{T_0 - T_1},\quad \vartheta \equiv \frac{v_b}{u_0},\quad \overline{u}_0 = \frac{u_0 b}{\kappa}. \tag{10}$$

We note that $\overline{u}_0$ has the physical meaning of the Péclet number, characterizing the ratio of the heat convection to heat conduction. In the dimensionless form we have

$$\overline{u}(\overline{x})\frac{\partial \overline{T}}{\partial \overline{x}} + \overline{v}(\overline{y})\frac{\partial \overline{T}}{\partial \overline{y}} = \frac{\partial^2 \overline{T}}{\partial \overline{x}^2} + \frac{\partial^2 \overline{T}}{\partial \overline{y}^2} + \frac{\partial^2 \overline{T}}{\partial \overline{x}^2}. \tag{11}$$

We solve Eq. (11) by the separation of variables. We assume a particulate solution in the form of a product $X(\overline{x})\,Y(\overline{y})\,Z(\overline{z})$. Substituting into Eq. (11) we find

$$\frac{X''}{X} - \overline{u}\frac{X'}{X} = -\frac{Y''}{Y} + \overline{v}\frac{Y'}{Y} - \frac{Z''}{Z}. \tag{12}$$

This equation will be satisfied for arbitrary independent variables if the functions X, Y, and Z satisfy the following ordinary differential equations

$$X'' - \overline{u}X' - \Lambda_x X = 0, \tag{13}$$

$$Y'' - \overline{v}Y' + \Lambda_y Y = 0, \tag{14}$$

$$Z'' + \Lambda_z Z = 0, \tag{15}$$

and the parameters $\Lambda_x, \Lambda_y, \Lambda_z$ are related as $\Lambda_x = \Lambda_y + \Lambda_z$. A general solution can be fond as a linear combination of independent partial solutions,

$$\overline{T}(\overline{x},\overline{y},\overline{z}) = \sum_{m>1}\sum_{n>1} C_{mn} X_{mn}(\overline{x}) Y_m(\overline{y}) Z_n(\overline{z}), \tag{16}$$

where X_{mn}, Y_m, Z_n are solutions to Eqs. (13), (14), and (15), respectively, for different values of parameters $\Lambda_{xmn} = \Lambda_{ym} + \Lambda_{zn}$.

A solution $\overline{T}(\overline{x},\overline{y},\overline{z})$ of Eq. (11) will be searched, satisfying the following boundary conditions:

$$\overline{T}(0,\overline{y},\overline{z}) = F(\overline{y},\overline{z}), \tag{17}$$

$$\overline{T}(\overline{a},\overline{y},\overline{z}) = 0, \tag{18}$$

$$\overline{T}(\overline{x},-1,\overline{z}) = \overline{T}(\overline{x},1,\overline{z}) = 0, \tag{19}$$

$$\overline{T}(\overline{x},\overline{y},-\overline{c}) = \overline{T}(\overline{x},\overline{y},\overline{c}) = 0. \tag{20}$$

We only consider cases, when the distribution of the temperatures at the inlet, given by function $F(\overline{y},\overline{z})$ is symmetric with respect to the axes $\overline{y},\overline{z}$. This allows considering only the intervals $0 \le \overline{y} \le 1,\ 0 \le \overline{z} \le \overline{c}$. The boundary conditions at $\overline{y} = -1,\ \overline{z} = -\overline{c}$ will be replaced by the requirements of symmetry—all odd derivatives must be zero, in particular

$$\left.\frac{\partial \overline{T}}{\partial \overline{y}}\right|_{\overline{y}=0} = 0,\ \left.\frac{\partial \overline{T}}{\partial \overline{z}}\right|_{\overline{z}=0} = 0. \tag{21}$$

Boundary conditions Eq. (19), (20), and (21) will be assured by requiring

$$Y_m'(0) = Y_n(1) = 0. \tag{22}$$

$$Z_n'(0) = Z_n(\overline{c}) = 0. \tag{23}$$

Boundary condition Eq. (18) will be satisfied for

$$X_{mn}(\overline{a}) = 0. \tag{24}$$

Further we chose

$$X_{mn}(0) = 1. \tag{25}$$

so that boundary condition (17)

$$\sum_{m\ge1}\sum_{n\ge1} A_{mn} Y_m(\overline{y}) Z_n(\overline{z}) = F\left(\overline{y},\overline{z}\right). \tag{26}$$

The coefficients A_{mn} are chosen in the way that this condition holds. We consider a simpler case when the right-hand side of Eq. (26) can be expressed as a product of two functions,

$$F\left(\overline{y},\overline{z}\right) = F_y(\overline{y}) F_z(\overline{z}),\ F_y(\overline{y}) = \sum_{m\ge0} B_m Y_m(\overline{y}),\ F_z(\overline{z}) = \sum_{n\ge0} C_n Z_n(\overline{z}). \tag{27}$$

Then the coefficients A_{mn} are given as $A_{mn} = B_m C_n$. We come back to the determination of the coefficients B_m and C_n after solving the differential equations (13) to (15).

Eq. (15) can easily be solved. For the symmetric case it is sufficient to consider solution

$$Z = C\cos\Lambda_z^{1/2}\overline{z}, \quad \Lambda_z^{1/2} = \frac{(2n-1)\pi}{2\overline{c}}, \quad n = 1,2,3,\ldots \,. \tag{28}$$

Substituting $\overline{v} = \overline{u}_0\vartheta\overline{y}$ for the symmetric case, Eq. (14) reads

$$Y'' - \overline{u}_0\vartheta\overline{y}Y' + \Lambda_y Y = 0\,. \tag{29}$$

To transform this equation to a standard form, we substitute

$$\overline{y} \equiv -\frac{\overline{u}_0\vartheta}{2}t^2, \quad W_y = Ye^t\,. \tag{30}$$

This substitution results into Kummer's equation [Abramowitz 1964]

$$tW_y'' + (\beta_y - t)W_y' - \alpha_y W_y = 0, \;\; \alpha_y = \frac{1}{2}\left(1 + \frac{\Lambda_y}{\overline{u}_0\vartheta}\right), \quad \beta_y = \frac{1}{2}. \tag{31}$$

Solution of Kummer's equation can be given in terms of Kummer's (confluent hypergeometric) functions *M* and *U*:

$$W_y = A_y M\left(\alpha_y,\beta_y,t\right) + B_y U\left(\alpha_y,\beta_y,t\right). \tag{32}$$

A solution, satisfying initial conditions $Y(0) = 1, \;\; Y'(0) = 0$ is

$$Y = e^{-t}M\left(\alpha_y,\beta_y,t\right). \tag{33}$$

Further we proceed to Eq. (13), which we will solve for boundary conditions

$$X(0) = 1, \;\; X(\overline{a}) = 0\,. \tag{34}$$

It is necessary to determine the parameter Λ_y such that the second condition (22), $Y(1) = 0$, holds.

Substituting $\overline{u} = \overline{u}_0\left(1 - \vartheta\overline{x}\right)$ for the symmetric case, reads

$$X'' - \overline{u}_0\left(1 - \vartheta\overline{x}\right)X' - \Lambda_x X = 0\,. \tag{35}$$

This equation can also be transformed to the Kummer's equation (31) using

$$s = -\frac{\overline{u}_0}{2\vartheta}\left(1 - \vartheta\overline{x}\right)^2, \quad W_x = Ye^s\,. \tag{36}$$

The parameters of the solution are

$$\alpha_x = -\frac{\Lambda_x}{2\overline{u}_0\vartheta}, \quad \beta_x = \frac{1}{2}. \tag{37}$$

A general solution in the form (32) is not suitable, because the function *U* has complex values. This function can be expressed as

$$U\left(a,b,s\right) = \frac{\pi}{\sin\pi b}\left[\frac{M(a,b,s)}{\Gamma(1+a-b)\Gamma(b)} - z^{1-b}\frac{M\left(1-a-b,2-b,s\right)}{\Gamma(a)\Gamma(2-b)}\right]. \tag{38}$$

The functions M are real. The reason of the imaginary component is the power $s^{1-b} = s^{1/2}$, because s is negatie. We note that function $(-s)^{1/2} M\left(\alpha + \frac{1}{2}, \frac{3}{2}, s\right)$ is a solution linearly independent of $M\left(a, \frac{1}{2}, s\right)$ and it is real for the present case. Therefore, it is convenient to assume the solution in the form

$$X(t) = A_x X_A(s) + B_x X_B(s) \tag{39}$$

where $X_1(s) \equiv M\left(\alpha_x, \frac{1}{2}, s\right)$ and $X_2(s) \equiv (-s)^{1/2} M\left(\alpha_x + \frac{1}{2}, \frac{3}{2}, s\right)$. In order to satisfy boundary conditions (34), the constants are chosen as follows:

$$A_x = X_B(q)/D,\ B_x = X_A(q)/D,\ D \equiv X_A(0)X_B(q) - X_A(q)X_B(0), \tag{40}$$

$$q \equiv -\frac{\overline{u}_0}{2\vartheta}(1 - \vartheta\overline{a})^2. \tag{41}$$

We determine now coefficients B_m and C_n. Specially we consider the case of homogeneous inlet temperature, corresponding to setting $F_y = 1$ for $\overline{y} \in (0,1)$ and $F_z = 1$ for $\overline{z} \in (0,\overline{c})$. However, with respect to boundary conditions (22) and (23) these functions must vanish at the endpoints of the respective intervals: $F_y(1) = 0$, $F_z(\overline{c}) = 0$ and be even functions. The last requirement was already included in choosing the solutions Eqs. (28) and (33). Coefficients for the cosines series C_m are determined by Fourier analysis of the square signal as $C_m = \frac{4}{(2n-1)\pi}(-1)^{n-1}$. The coefficients B_m are obtained by minimizing the residuum $R_y = \int_0^1 \left[\sum_{n=1}^{n_{\max}} B_n Y_n(t) - 1\right]^2 dt$. The necessary conditions of a minimum is

$$\frac{\partial R_y}{\partial B_{n'}} = \int_0^1 Y_{n'}(t)\left[\sum_{n=1}^{n_{\max}} B_n Y_n(t) - 1\right] dt = 0,\ n' = 1,...,n_{\max}. \tag{42}$$

After a re-arrangement we obtain a set of linear equations

$$\sum_{n=1}^{n_{\max}} G_{n'n} B_n = g_{n'},\quad n' = 1,...,n_{\max},\ G_{n'n} \equiv \int_0^1 Y_{n'}(t) Y_n(t) dt,\quad g_{n'} \equiv \int_0^1 Y_{n'}(t) dt. \tag{43}$$

4. Numerical computations and results

The computation model in the commercial software Fluent for CFD simulation was created according to the experimental design in order to verify the setup, especially the efficiency of the input screen. The purpose of the screen is to form a uniform velocity field at the inlet to the chamber. The flow was modeled as time independent. The gas (nitrogen) was assumed to be incompressible and the heating due to the viscous friction in liquid could be neglected. We solved completely the balances of mass, momentum and energy with the restrictions mentioned above. A section of the geometrical model is in Figure 2. The flow enters the domain on inlet, passing through the porous jump. This jump represents the screen used to

homogenize the flow deformed by the inlet pipes. Then the flow passes the second screen (porous jump) in the forward direction and up and down the porous medium simulating sintered glass plates. The inlet velocity was calculated from known flow-rate to be 1.66 m/s. The temperature of the inlet flow was set to 240 K. This temperature was also set for the walls of inlet parts. Because in reality all the inlet pipes are drilled into a cooper block cooled to temperature 240 K, the wall thickness for the heat conduction equation was set to zero. The flow temperature was thus equal to the wall temperature. The barometric pressure was set at the boundary condition outlet. The wall temperature at the horizontal and vertical walls of the chamber and at the outlet parts was set to 300 K. The ratio between the flow outgoing the vertical outlets and horizontal outlet were set with using the porous jump and porous media condition. Porous medium is modeled by the addition of a momentum source term to the standard fluid flow equations. The source term is composed of a viscous loss term and an inertial loss term. For a homogeneous porous media can the source term is formulated as

$$S_i = -\left(\frac{\mu}{\alpha} v_i + C_p \frac{1}{2} \rho v_{mag} v_i \right) \tag{44}$$

where μ is the laminar fluid viscosity, α is the permeability and C_2 is the inertial resistance factor. A simplification of Eq. (44) for the porous media in 1D is the porous jump

$$\Delta p = -\left(\frac{\mu}{\alpha} v + C_p \frac{1}{2} \rho v^2 \right) \Delta m \tag{45}$$

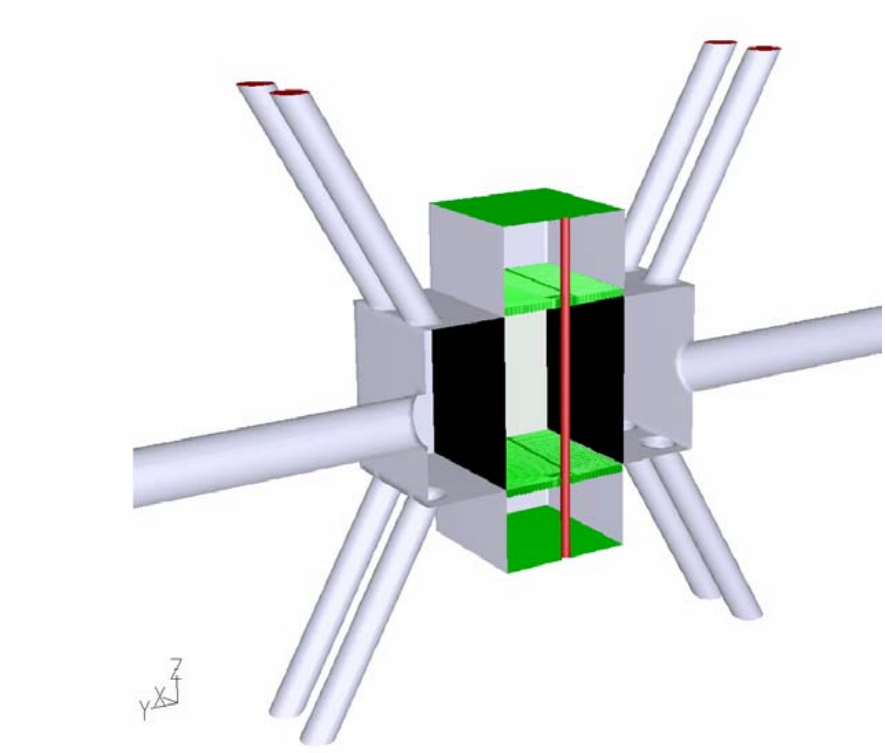

Figure 2.: Geometry of the computation model. This figure also shows the inlets (inclined channels) and outlets (wider horizontal channels). The flow enters either from left inlet channels and leaves through the outlet channel at right, or vice versa. The passive inlets and outlet are closed by an external valve.

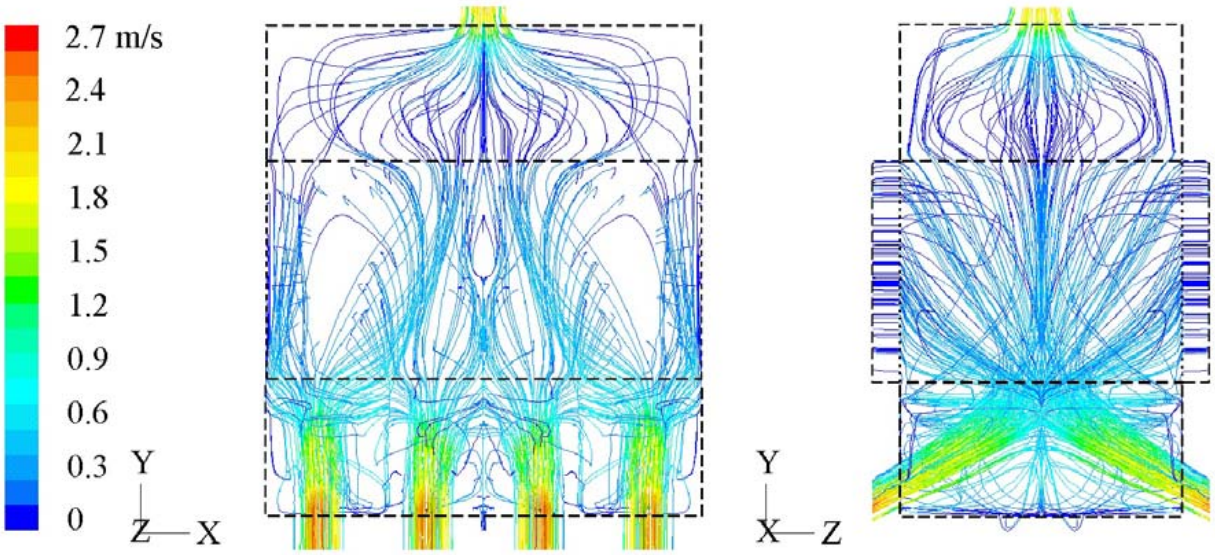

Figure 3: Streamlines at the central horizontal plane (left) and at the central vertical plane (right). Dashed lines are the inlet (lower) and outlet (upper) screens. It can be seen that the inlet screen does not homogenize the flow completely, although the main influence of the inlet pipes is filtered out.

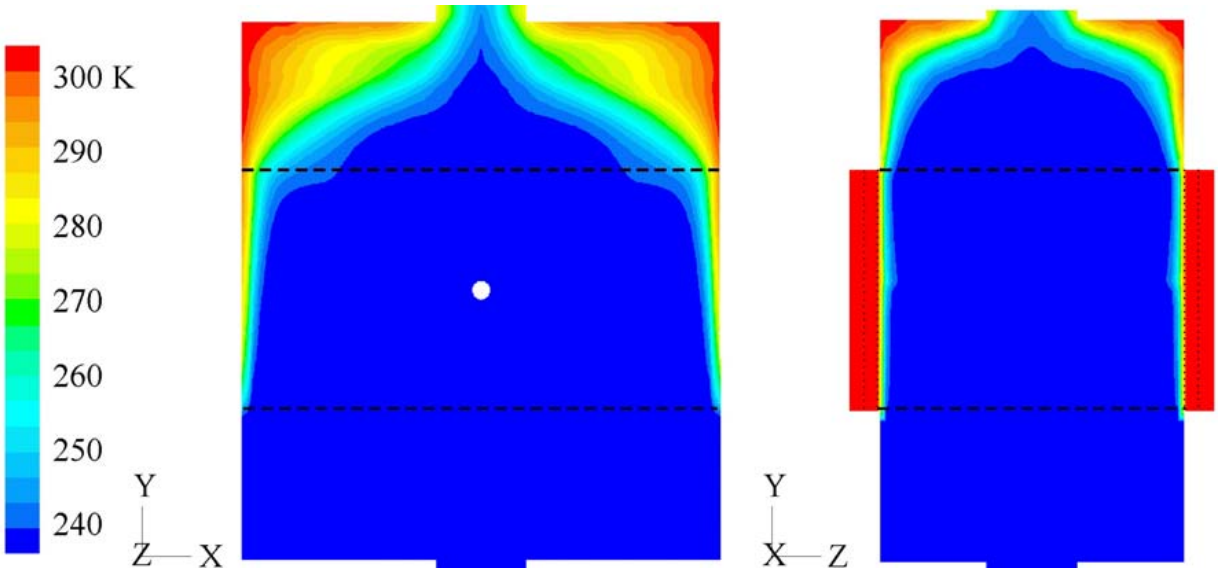

Figure 4: Temperature field at the central horizontal plane (left) and at the central vertical plane (right). Dashed lines are the inlet (lower) and outlet (upper) screens. It can be seen that the thermal boundary layer is substantially thinner in the case when it is sucked out through the sintered glass plates (right) in comparison to the normal thickening of the thermal boundary layer on the optical glass (left).

where Δm is the thickness of the medium. Due to the insignificant speed of flow into the computational domain, in our calculations, we neglected the second term in the brackets and estimated the value of α based on a known pressure loss. The constant temperature of 300 K was assigned to the porous media. The temperature at the glass wall was set at 300 K, corresponding to the surrounding temperature, with the glass thickness 2 mm. In this case the glass thickness cannot be neglected, due to the low heat conduction coefficient of glass.

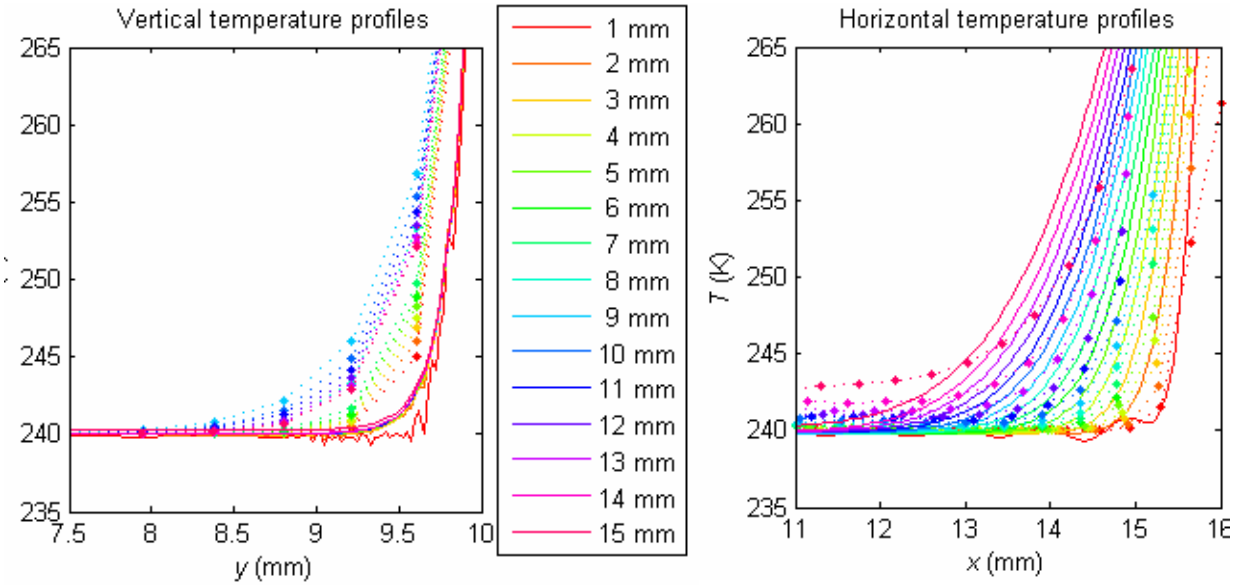

Figure 5: Temperature profiles in the vertical central plane (left) and in the horizontal central plane (right). Solid lines are computed using the analytical model, points connected by dotted lines are results of the CFD Fluent. The profiles are computed at given distances from the inlet screen (the distance of the inlet and outlet screens is 16 mm). Note that the boundary layer on the left is much thinner than on the right—due to the sucking effect.

5. Conclusions

The results indicate that the design objectives of the experimental device were met. However, there is a space for improvements. It appears that the inlet screen has a too small hydrodynamic resistance, allowing some disturbances from the inlet tubes to enter the measuring chamber. This causes an increase of the conductive heat transport from the hot walls and explains the difference between the numerical simulation and analytical computations.

Comparing the numerical and analytical computations methodically, the analytical computations have the obvious advantage of deeper insight into the basic mechanisms and influences of parameters. On the other hand, some simplifications must be accepted and it is not possible to capture important effect such as the disturbances protruding through the

screens. It is also to be said that in this 3D case—although with a simple geometry—the complexity of the analytical computations is almost prohibitive.

6. Acknowledgement

A support by Grant No. 101/05/2214 of the Grant Agency of the Czech Republic is gratefully acknowledged.

7. References

Cornell, W. G. (1958) Losses in flow normal to plane screens. *Trans. ASME,* 80, pp. 791-799.

Hacker, P. T. (1951) Experimental values of the surface tension of supercooled water. Technical Note 2510, National Advisory Committee for Aeronautics (1951), URL http://naca.larc.nasa.gov/reports/1951/naca-tn-2510/naca-tn-2%510.pdf.

Floriano, M. A. & Angel, C. A. (1990) Surface tension and molar surface free energy and entropy of water to -27.2°C. *Journal of Physical Chemistry* 94, pp. 4199-4202.

Abramowitz, M. & Stegun, I. A. (1964) *Handbook of mathematical functions.* Dover, New York.